

Gravi-magnetic anomalies of uniform thin polygonal sheets

Horst Holstein¹, Des Fitzgerald², Costas Anastasiades³

1. Aberystwyth University, UK, hoh@aber.ac.uk and Intrepid-Geophysics, Australia
2. Director, Intrepid-Geophysics, Australia, des@intrepid-geophysics.com
3. Aberystwyth University, UK, cpa05@aber.ac.uk

ABSTRACT

Thin planar sheets are useful gravitational and magnetic models of dykes and veins treated as two-dimensional geophysical structures on the survey scale. Thus, the anomaly of a planar polygonal thin sheet of uniform surface density or magnetization in arbitrary orientation has practical interest. The limiting thin-sheet anomaly can be approached from the corresponding polyhedral parallelepiped under decreasing thickness, though the numerical limit cannot be reached this way on account of the floating point finite precision.

We derive the analytical zero thickness limit for the gravity potential while maintaining finite total mass. We use the concept of gravi-magnetic similarity to extend the thin-sheet potential formula to include the potential, field and field gradient in both gravity and magnetic cases, thereby generalising other studies that have obtained isolated polygonal thin-sheet anomaly solutions. We compare the anomalies computed by the new formulae to those of corresponding finite thickness targets, and to the finite difference estimates of the field and field gradient obtained from numerically differentiated thin-sheet potentials. In both cases a second order rate of approach to the limit is observed, verifying the correctness of the new formulae.

Thin-sheet solutions are attractive for their reduced computational burden compared to full parallelepiped solutions, while the stacking of thin sheets may be used to simulate variable density or magnetization targets. It is anticipated that thin-sheet solutions presented here will find wide application in gravi-magnetic modelling.

Key words: thin sheet, modeling, gravity, magnetics, potential theory, tensors.

INTRODUCTION

Thin-sheet targets are useful models for finite-strike dykes and veins, resolved only as two-dimensional in the scale of a particular gravity or magnetic survey (Grant and West, 1965). As stacked laminae they can approximate three dimensional targets with varying material properties (Talwani and Ewing, 1960). Together with their reduced computational burden over a full polyhedral calculation they are a natural model choice in stochastic inversion (Wildman and Gazonas, 2009).

The thin-sheet studies above use *ad hoc* derivations, giving no indication of how the formulae are related to each other. Strakhov *et al.* (1986) first demonstrated the striking similarity among the polyhedral gravity and magnetic anomaly formulae, and indicated the same for the thin-sheet formulae, without giving full details. Their derivation in terms of complex variable theory is somewhat unnatural. A simple vector/tensor derivation for the polyhedral anomalies was given by Holstein (2002a), and the present paper makes the extension to thin sheets. As well as expressing the gravi-magnetic thin-sheet anomalies in a single framework, we include

a new result for the magnetic field gradient tensor of a uniformly magnetized thin sheet.

Our derivation considers the parallelepiped gravity potential anomaly a as a function its thickness T , and seeks an analytical expression for the limit of the anomaly per unit thickness, $a(T)/T$, as T tends to zero. This is equivalent to differentiation, but explicit differentiation is not necessary, since the polyhedral anomaly formulae form a known derivative hierarchy. We simply take the appropriate terms from the next order of anomaly. Only for the magnetic field gradient thin-sheet formula do we need a new differentiated result, but by then all terms are algebraic and explicit final differentiation is easy to perform. In summary, the entire set of gravi-magnetic thin-sheet formulae largely reuses the functions employed in the known polyhedral anomaly solutions, thus preserving similarity and aiding analysis.

We verify the thin-sheet formulae by comparison with finite thickness parallelepiped cases of decreasing thickness T , and with the numerically differentiated thin-sheet potential anomaly to approximate the field and field gradient for decreasing step length t . We find

the finite forms approach the limiting thin-sheet forms with second order accuracy $O(T^2), O(t^2)$ respectively, confirming the validity of our thin-sheet formulae.

A synthetic survey over a 41 by 41 mesh showed that the thin-sheet formulae were computed more than twice as fast as the corresponding finite-thickness polyhedral parallelepiped formulae, supporting our conclusion that the thin-sheet formulae can be used to advantage in the modelling of 2D gravity and magnetic targets.

GOVERNING EQUATIONS

Consider an arbitrarily orientated parallelepiped with one plane polygonal non-thin surface $ABCD...$ designated as 'top', the partnering surface $A'B'C'D'$... designated as 'bottom', while $B'C'CB$ designates the 'front' surface abutting top edge BC , as shown in the geometry of Figure 1.

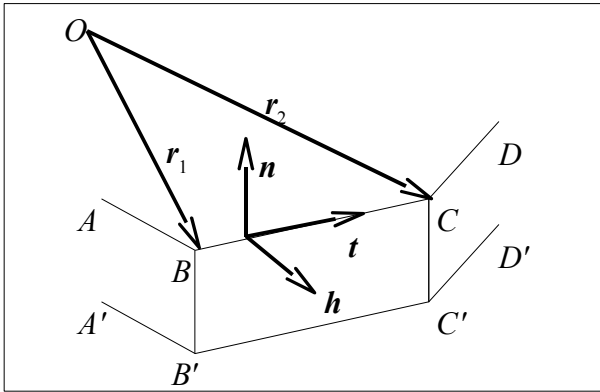


Figure 1. Part of a parallelepiped model, showing a top facet edge orthonormal vector triad (h, t, n) . In the limiting thin-sheet case, short edges $B'B$, $C'C$, ... shrink to zero.

The unit outward normal vector to facet $ABCD...$ is designated by n , and edge BC of the top facet defines an orthonormal triad (h, t, n) , such that h is pointing horizontally outward from the facet plane, perpendicular to edge BC , and t is directed tangentially along edge BC in an anticlockwise sense around the outward facet normal n . Vertices B and C have position vectors r_1 and r_2 relative to the observation point O .

More generally, we add the subscript i to identify a particular facet, and the subscript pair ij to identify edge j of facet i . Vectors r_{ij1} and r_{ij2} are the position vectors to vertices 1 and 2 of edge ij . These correspond to vectors OB and OC in Figure 1 when i denotes the top facet and ij the top edge BC . Each edge ij of each facet i has its own orthonormal vector triad (h_{ij}, t_{ij}, n_i) , relative to which horizontal and vertical projections of the vertex position vectors are

$$h_{ij} = r_{ij1} \cdot h_{ij} = r_{ij2} \cdot h_{ij}, \quad v_i = r_{ij1} \cdot n_i = r_{ij2} \cdot h_{ij} \quad (1)$$

while the lateral projections are

$$l_{ij1} = r_{ij1} \cdot t_{ij}, \quad l_{ij2} = r_{ij2} \cdot t_{ij}, \quad \bar{l}_{ij} = (l_{ij1} + l_{ij2})/2 \quad (2)$$

The horizontal projections do not distinguish between the vertices, and the vertical projection is common to all vertex position vectors of the facet. In those situations, we denote the vectors by r_{ij} and just r_i . The gravity potential, field and field gradient φ_g, f_g, G_g and magnetic potential, field and field gradient φ_m, f_m, G_m are then respectively (Holstein 2002a,b)

$$\varphi_g = \frac{1}{2} G \rho \sum_i r_i \cdot n_i \sum_j b_{ij} \cdot r_{ij} \quad (3)$$

$$f_g = \nabla \varphi_g = -G \rho \sum_i n_i \sum_j b_{ij} \cdot r_{ij} \quad (4)$$

$$G_g = \nabla f_g = G \rho \sum_i n_i \sum_j b_{ij} \quad (5)$$

$$\varphi_m = -\sum_i \mu \cdot n_i \sum_j b'_{ij} \cdot r_{ij} \quad (6)$$

$$f_m = \nabla \varphi_m = \sum_i \mu \cdot n_i \sum_j b_{ij} \quad (7)$$

$$G_m = \nabla f_m = -\sum_i \mu \cdot n_i \sum_j b'_{ij} \quad (8)$$

where $G \rho$ is the constant of universal gravitation times the density, μ is the vector of magnetization, and b_{ij} is a vector function in the (n_i, h_{ij}) plane encapsulating the Newtonian potential for edge ij . The recurrence of the functions b_{ij} in equations (3)-(7) expresses the gravi-magnetic similarity for polyhedral targets. Only equation (8) requires a new term b'_{ij} , equal to the tensor $-\nabla b_{ij}$. A formula for b_{ij} is

$$b_{ij} = 2 h_{ij} \operatorname{arctanh} \Lambda_{ij} - 2 n_i^s \operatorname{arctan} \lambda_{ij} \quad (9)$$

where, omitting subscripts ij for a top edge (e.g. BC in Figure 1) of length L ,

$$\Lambda = L/(2\bar{r}), \quad \bar{r} = (|r_1| + |r_2|)/2,$$

$$n^s = n \operatorname{sign}(v), \quad \lambda = \frac{h\Lambda}{\bar{r}(1-\Lambda^2) + |v|} \quad (10)$$

and v and h are defined in equation (1). The inner sum in equation (3) satisfies (Holstein, 2002a)

$$\sum_j b_{ij} \cdot r_{ij} = \int_{S_i} dS/r, \quad (11)$$

that is, the sum over the edge terms of a facet is equal to its area integral weighted by the reciprocal scalar distance from the observation point. Formulae (3)-(11) will now be adapted to the thin-sheet case.

The gravity potential thin-sheet anomaly

The Newtonian gravity potential of a target of volume V is given by the weighted volume integral

$$\varphi_g = G \rho \int_V dV/r \quad (12)$$

In the case of a thin sheet of constant thickness T , the volume element becomes $dV = T dS$, where dS is an element of surface. The limiting anomaly per unit thickness is then given by

$$\lim_{T \rightarrow 0} (\varphi_g/T) = G \rho \int_S dS/r \quad (13)$$

where the integration is carried out over the surface S of the sheet.

In practice, we shall retain a finite thickness parameter T in the formula so as to allow the target to have a finite volume and mass. Thus we express the thin-sheet gravity potential anomaly as

$$\varphi_g = G \rho T \int_S dS/r \quad (14)$$

When the surface S is a planar polygon, equation (11) applies, and thus the thin-sheet potential is given by

$$\varphi_g = G \rho T \sum_j \mathbf{b}_j \cdot \mathbf{r}_j \quad (15)$$

All subscripted quantities are expressed in the notation for the top facet (omitting the assumed first subscript $i=\text{top}$), except that the quantities are defined on the zero-thickness mid-plane of the thin sheet. Once again, only the edge functions \mathbf{b}_j are involved, without introducing any new functions. Consequently, gravi-magnetic similarity is found to apply also to the case of thin polygonal targets.

The gravity field thin-sheet anomaly

Remarkably, expression (15) for the thin-sheet gravity potential φ_g is the top facet term in the polyhedral gravity field expression (4). As a consequence, its gradient, the gravity field of the thin-sheet anomaly, is by reference to equation (5) given by

$$\mathbf{f}_g = \nabla \varphi_g = -G \rho T \sum_j \mathbf{b}_j \quad (16)$$

If only the component of gravity perpendicular to the plane of the thin-sheet target is required (for example, the vertical component of gravity in the case of a horizontal lamina), equations (9), (10) and (16) yield

$$\mathbf{f}_g \cdot \mathbf{n} = G \rho T \text{sign}(v) 2 \sum_j \arctan \lambda_j \quad (17)$$

Formally, this is the result of Talwani and Ewing (1960), although our form uses half the number of trigonometric function evaluations. An early version of equation (16) was obtained by Ketteridge (1996), using a limiting process on the polyhedral prism solution as the thickness T tends to zero.

The gravity gradient thin-sheet anomaly

The gradient of the gravity field solution (16) gives the gravity field gradient \mathbf{G}_g for the thin sheet,

$$\mathbf{G}_g = \nabla \mathbf{f}_g = G \rho T \sum_j \mathbf{b}'_j \quad (18)$$

where the tensor elements of $\mathbf{b}'_j = -\nabla \mathbf{b}_j$ are given in Holstein *et al.* (2007). Thus we find for the edges j of the top facet

$$\mathbf{b}'_j = (\mathbf{h}_j \mathbf{h}_j - \mathbf{n} \mathbf{n}) d_j + (\mathbf{h}_j \mathbf{t}_j + \mathbf{t}_j \mathbf{h}_j) e_j / 2 + (\mathbf{h}_j \mathbf{n} + \mathbf{n} \mathbf{h}_j) f_j \quad (19)$$

where

$$d_j = \frac{-2 \Lambda_j}{(1 - \Lambda_j^2)} \frac{h_j}{r_{j1} r_{j2}}, e_j = \frac{-2 \Lambda_j \bar{l}_j}{r_{j1} r_{j2}}, \quad (20)$$

$$f_j = \frac{-2 \Lambda_j}{(1 - \Lambda_j^2)} \frac{v}{r_{j1} r_{j2}}$$

The magnetic thin-sheet potential and field anomalies

By Poisson's relation, the magnetic thin-sheet potential φ_m is obtained from the corresponding gravity field (18) with adjustment of the physical parameters,

$$\varphi_m = \mu \cdot \mathbf{f}_g / (G \rho) \quad (21)$$

Similarly, the magnetic field \mathbf{f}_m is obtained from the gravity field gradient tensor (18)-(20),

$$\mathbf{f}_m = \mu \cdot \mathbf{G}_g / (G \rho) \quad (22)$$

The magnetic gradient thin-sheet anomaly

In the absence of a corresponding gravity result, we compute this anomaly from the gradient of the magnetic field anomaly. Thus

$$\mathbf{G}_m = \nabla \mathbf{f}_m \quad (23)$$

From equations (18), (22) and (23), we can write

$$\mathbf{G}_m = -T \mu \cdot \sum_j \mathbf{b}''_j \quad (24)$$

where

$$\mathbf{b}''_j = (\mathbf{h}_j \mathbf{h}_j - \mathbf{n} \mathbf{n}) \mathbf{d}'_j + (\mathbf{h}_j \mathbf{t}_j + \mathbf{t}_j \mathbf{h}_j) \mathbf{e}'_j / 2 + (\mathbf{h}_j \mathbf{n} + \mathbf{n} \mathbf{h}_j) \mathbf{f}'_j \quad (25)$$

and

$$\mathbf{d}'_j = -\nabla d_j, \mathbf{e}'_j = -\nabla e_j, \mathbf{f}'_j = -\nabla f_j \quad (26)$$

The three vectors, expressed in the local $(\mathbf{h}_j, \mathbf{t}_j, \mathbf{n})$ frame of the top edge, can be assembled into the three columns of a 3 by 3 matrix \mathbf{A} . This matrix is symmetric and has trace zero. Direct differentiation gives

$$A_{11} = (h^2 Q - r_1 r_2) V \quad (27)$$

$$A_{22} = (\bar{l}^2 (R - \Lambda^2) - r_1 r_2) U \quad (28)$$

$$A_{33} = (v^2 Q - r_1 r_2) V \quad (29)$$

$$A_{12} = A_{21} = h \bar{l} P U \quad (30)$$

$$A_{13} = A_{31} = h v Q V \quad (31)$$

$$A_{23} = A_{32} = \bar{l} v (R + \Lambda^2) V \quad (32)$$

where

$$P = 1 + r_1 / r_2 + r_2 / r_1 \quad (33)$$

$$Q = P + 2 \Lambda^2 / (1 - \Lambda^2) \quad (34)$$

$$R = P - \bar{l}^2 / (r_1 r_2) \quad (35)$$

$$U = 2 \Lambda / (r_1 r_2)^2 \quad (36)$$

$$V = U / (1 - \Lambda^2) \quad (37)$$

and where the subscript j associated with edge j of the top facet has been omitted for clarity, from quantities h, \bar{l}, r_1, r_2 and Λ . Vectors $\mathbf{d}', \mathbf{e}', \mathbf{f}'$ are then

$$\mathbf{d}' = -\nabla d = \mathbf{h} A_{11} + \mathbf{t} A_{21} + \mathbf{n} A_{31}$$

$$\mathbf{e}' = -\nabla e = \mathbf{h} A_{12} + \mathbf{t} A_{22} + \mathbf{n} A_{32} \quad (38)$$

$$\mathbf{f}' = -\nabla f = \mathbf{h} A_{13} + \mathbf{t} A_{23} + \mathbf{n} A_{33}$$

A term such as $\mu \cdot (\mathbf{h} \mathbf{h} - \mathbf{n} \mathbf{n}) \mathbf{d}'$ arising in equation (25) via equation (24) is computed as a rank 2 tensor, whose 3 by 3 matrix is expressed via column and row $(\cdot)^T$ vectors by $(\mu^T \mathbf{h})(\mathbf{h} \mathbf{d}'^T) - (\mu^T \mathbf{n})(\mathbf{n} \mathbf{d}'^T)$. Symmetry permits also a post inner product in equation (25), leading to terms such as $(\mathbf{h} \mathbf{h} - \mathbf{n} \mathbf{n})(\mathbf{d}' \cdot \mu)$ with more attractive matrix computation $(\mathbf{h} \mathbf{h}^T - \mathbf{n} \mathbf{n}^T)(\mathbf{d}'^T \mu)$.

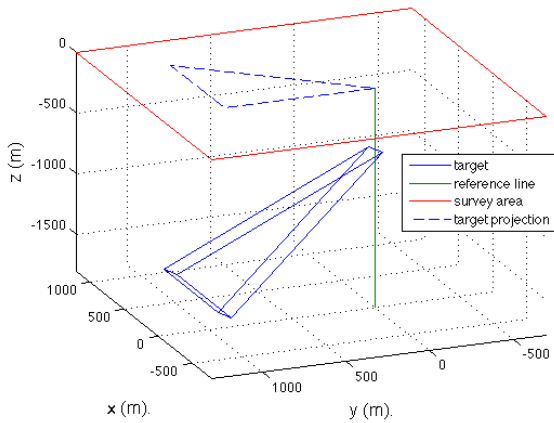


Figure 2. Thin target model used for synthetic modelling. Mid-plane vertices are at $(0,0,-500)$, $(0,900,-1700)$, $(800,900,-1700)$. A vertical reference line is drawn to the surface point $(0,0,0)$. The projection of the target mid-plane on to the 2000m by 2000m survey area in the plane $z=0$ is also shown.

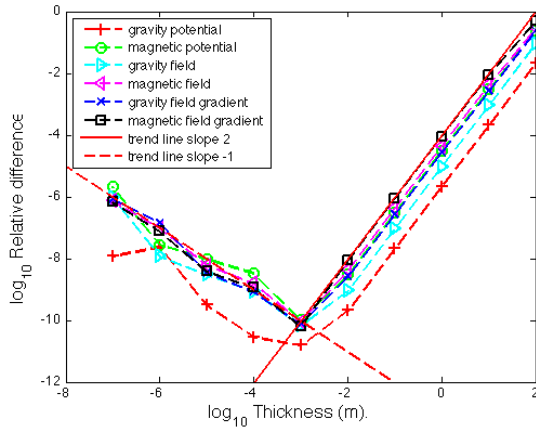


Figure 3. Relative difference between a target of finite thickness and its limiting thin form for the potential, field and gradient in the gravity and magnetic cases observed at point $(0,0,0)$.

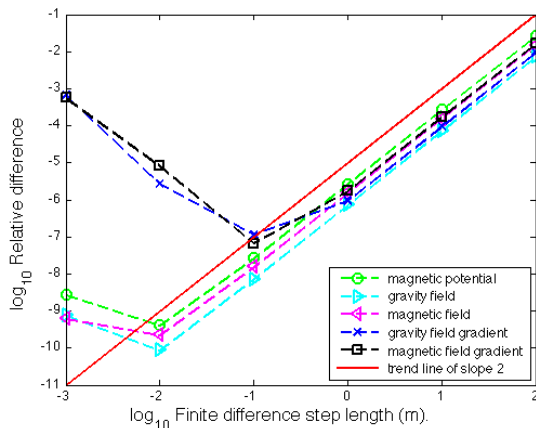


Figure 4. Relative difference between limiting thin-sheet anomalies and their finite difference potential derivative estimates, evaluated at observation point $(0,0,0)$.

VERIFICATION OF THE FORMULAE

The relationship between an anomaly $a(T)$ computed for a target of finite thickness and the zero-thickness case can be explored by the Taylor series around $T=0$,

$$a(T) = T \frac{\partial a}{\partial T} + \frac{T^2}{2} \frac{\partial^2 a}{\partial T^2} + O(T^3) \quad (39)$$

in which $a(0) = 0$. The term $a(T)/T$ is the anomaly per unit target thickness for finite thickness T , which tends to $\partial a / \partial T$ as $T \rightarrow 0$ by l'Hopital's rule. This is the quantity expressed by our limiting thin-sheet formulae. The normed relative difference between the finite and limiting cases expressed by the left hand side of

$$\left\| \frac{a(T)}{T} - \frac{\partial a}{\partial T} \right\| \left\| \frac{\partial a}{\partial T} \right\|^{-1} = \left| \frac{T}{2} \right\| \left\| \frac{\partial^2 a}{\partial T^2} \right\| \left\| \frac{\partial a}{\partial T} \right\|^{-1} + O(T^2) \quad (40)$$

is therefore suitable for tracking the approach of the finite and limiting thin cases as $T \rightarrow 0$.

We have computed the left hand side of equation (40) for each of the six gravi-magnetic anomalies, evaluated at the observation point $(0,0,0)$ for the triangular target shown in Figure 2. The finite thickness cases are computed with polyhedral codes for the gravi-magnetic anomalies. The results are shown in Figure 3 on a log-log scale, in which the observed initial slope of 2 reveals an initial quadratic convergence between finite and limiting thin cases. It suggests that $a(T)$ has only odd powers in the Taylor series (39). As the thickness decreases, the trend line is found to change from a slope 2 to a slope of -1, indicating a divergence of $a(T)/T$ from the thin-sheet formulae. Divergence is expected on account of finite precision arithmetic rounding error. On the basis of Figure 3, we can state that the limiting thin-sheet formulae are correct because the finite cases approach them with an anticipated power law. The figure also demonstrates the numerical instability in attempting to approach the limiting form by standard polyhedral codes alone (compare Holstein *et al.*, 2008).

A second test concerns the internal consistency of the limiting thin-sheet equations, which require the Cartesian derivatives of the potentials to yield the field and field gradients in the gravity and magnetic cases. To this end, we evaluate the limiting thin-sheet gravity and magnetic potential anomalies at points (ξ, η, ζ) in the neighbourhood of the observation point $(0,0,0)$, where each of ξ, η, ζ takes on values 0 and $\pm t$, for decreasing values of step length t . Thereby, central difference estimates are obtained for the potential derivatives

$\Phi_{g,x}, \Phi_{g,y}, \Phi_{g,z}, \Phi_{g,xx}, \Phi_{g,xy}, \dots, \Phi_{g,zz}, \Phi_{m,x}, \dots, \Phi_{m,zz}$ from which finite difference fields and gradients can be reconstructed. We expect the numerically estimated anomalies to have a relative error proportional to t^2 , compared to their exact limiting thin-sheet forms. This

is confirmed in Figure 4. At decreasing step length, the finite difference anomalies approach the limiting formulae quadratically, as evidenced by the initial slope 2 in the log-log graph. The gravity and magnetic field gradients are the first to depart from this trend at decreasing step length. This is expected, since their finite difference derivative estimates require second order differences, which are more prone to rounding error than the first order differences of finite precision data. This test demonstrates the separate consistencies of the gravity and magnetic thin-sheet formulae, with respect to the gravity and magnetic potential formulations, respectively. However, the gravity and magnetic cases themselves are linked by Poisson's relation, as shown by equations (21) and (22), so we have shown the entire limiting thin-sheet anomaly formula set, from gravity potential to magnetic field gradient, to be consistent with the thin-sheet gravity potential formulation.

Finally, we present in Figure 5 a synthetic survey over the target and observation plane of Figure 2. The limiting thin-sheet formula for the magnetic field gradient was used, with thickness parameter $T=100\text{m}$ (c.f. equation (24)). Other defining parameters are given in the Figure captions. The six limiting thin-sheet gravi-magnetic anomalies were computed on a 41 by 41 grid, simulating line spacings of 50m in the x and y directions. Only results for the magnetic field gradient are shown.

The time taken to compute the entire gravi-magnetic anomaly set over the whole grid was 1.82s in a Matlab environment. This compares with 3.99s used for the full polyhedral solution for the parallelepiped of 100m thickness. At the resolution presented in Figure 5, differences between the limiting thin-sheet and the parallelepiped magnetic gradient calculations are not readily evident.

For every top edge visited in the limiting thin-sheet algorithm, the full polyhedral case must visit six edges, corresponding to itself and the bottom edge, and four edges of the thin adjacent side facet abutting top and bottom facets, as evident from Figure 1. Our polyhedral code is already optimized to share information on edges common to adjacent facets, so that the polyhedral overhead over the thin-sheet case may be closer to 3 than 6. We found a more modest gain of 2.2, suggesting that a speed-up of 3 applies to about 75 per cent of the thin-sheet code. Further optimization of our code may be possible.

All the code and tests were replicated in C++ on Windows/LINUX and on 32/64 bit hardware, as part of the general Intrepid libraries. Better efficiencies have resulted where some of the operations and variables are moved to purpose built objects and classes e.g. Tensor, Quaternions and Rotation Matrix classes (FitzGerald *et al.*, 2009). Opportunities exist for the compiler to add

optimizations such as inlining and threading. The real test of efficiency comes when very large fine resolution 3D models are constructed. The intention here is to use such code in the context of stochastic perturbations of both the geometry and the lithological properties.

CONCLUSIONS

Modelling of thin geological structures as limiting thin-sheet bodies is appropriate in many survey situations, where the survey scale cannot adequately resolve such targets as three dimensional. We present a set of formulae giving the potential, field and field gradient in the gravity and magnetic cases when such targets have uniform density or magnetization. The formulae have a close affinity to the finite thickness polyhedral case, and this fact allowed a ready derivation of the limiting thin-sheet formulae, in a common, uniform notation. Only in the magnetic gradient case were new relations required that were not already available from the full polyhedral case, and these were derived in this work. The resulting thin-sheet formulae exhibit the property of gravi-magnetic similarity, which allows them to be programmed efficiently in a single program with much reuse of the terms. Thus we offer a superior formulation that strongly emphasises commonality, and also provide a new result for the case of the magnetic gradient.

The implicit differential relationships between the formulae was used to verify the correctness of the formulae, further confirmed by an asymptotic approach of the full polyhedral anomaly formulae to the limiting cases.

In summary, this work provides a set of modelling formulae that will be useful in the interpretation of gravity and magnetic survey data. It will form part of the next version of the Geomodeller geophysics computation engine. The anticipated reduction in work load by a factor of between 3 and 6 in a section of the code more than doubled the speed over the full polyhedral case in the Matlab version, with even higher efficiencies found in the C++ version. The issue of validating the Full Tensor Magnetic Gradient code when remanence is involved has not yet been tackled, and remains a topic for further investigation.

ACKNOWLEDGMENTS

We thank Phil McInerney and Alan Reid for helpful discussions. The work was in part funded by support from the Australian Government Commercial Ready Grant program.

REFERENCES

Fitzgerald, D., Argast, D. and Holstein, H., 2009, Further developments with full tensor gradiometry datasets: 20th ASEG Geophysical Conference, Adelaide.
 Grant, F.S. and West, G.F. 1965, Interpretation theory in applied geophysics: McGraw-Hill.
 Holstein, H., 2002a, Gravimagnetic similarity for uniform polyhedra: *Geophysics*, **67**, 1126-1133.
 Holstein, H., 2002b, Invariance in gravimagnetic formulas for uniform polyhedra: *Geophysics*, **67**, 1134-1137.
 Holstein, H., Anastasiades, C. and Ketteridge, B., 2008, Gravimagnetic anomaly formulae for extended homogeneous prisms: 71st EAGE Conference & Exhibition, Saint Petersburg, Russia.
 Holstein, H., Sherratt, E.M. and Reid, A.B., 2007, Gravimagnetic field tensor gradiometry formulas for uniform polyhedra: 77th Conference & Exhibition of the SEG, San Antonio, Texas.

Ketteridge, B.T., 1996, Optimisation of geophysical investigation methods: Ph.D. Thesis, University of Wales, Aberystwyth.
 Strakhov, V.N., Lapina, M.I. and Yefimov, A.B., 1986, A solution to forward problems in gravity and magnetism with new analytical expressions for the field elements of standard approximating bodies I: *Izvestiya, Earth Sciences*, **22**, 471-482.
 Talwani, M. and Ewing, M., 1960, Rapid computation of gravitational attraction of three-dimensional bodies of arbitrary shape: *Geophysics*, **35**, 203-225.
 Wildman, R.A. and Gazonas, A., 2009, Gravitational and magnetic anomaly inversion using a tree-based geometry representation: *Geophysics*, **74**, I23-I35.

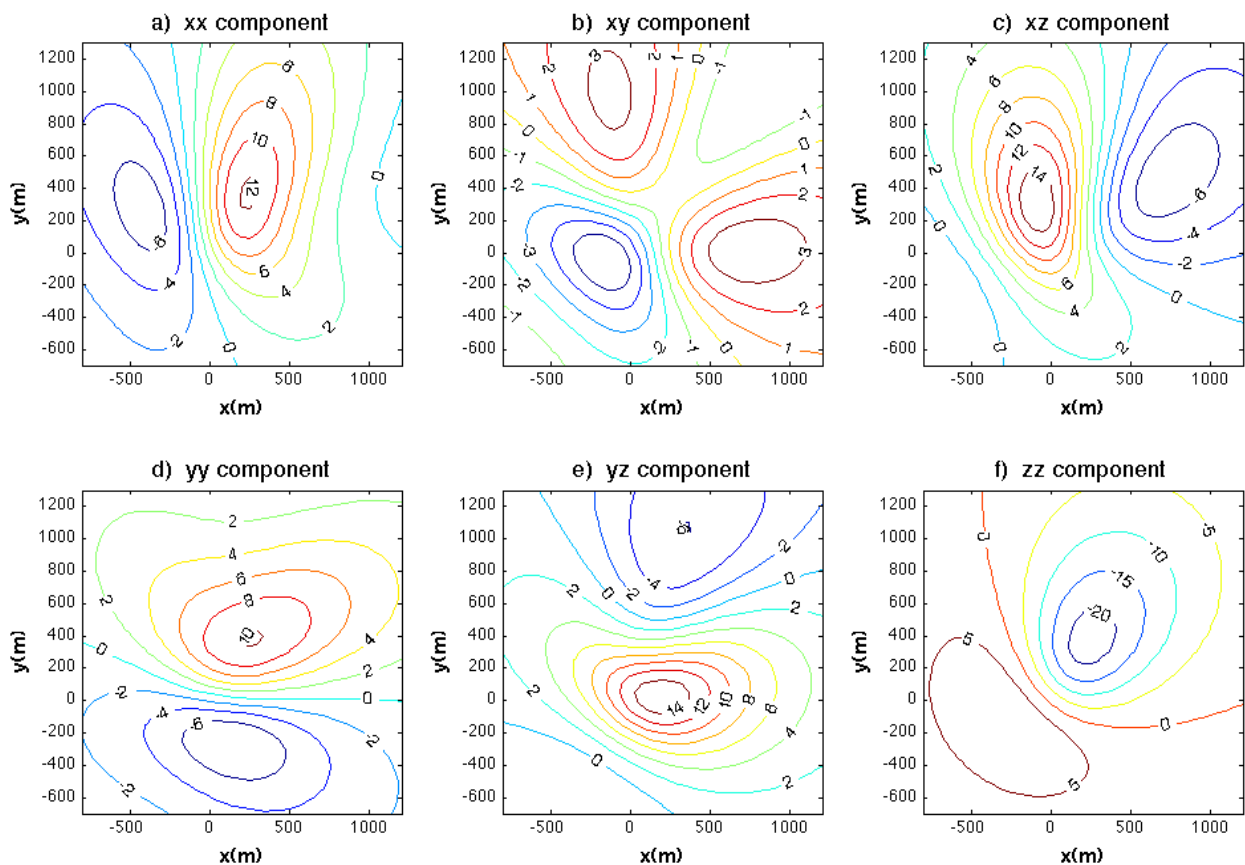


Figure 5. Limiting thin-sheet magnetic field gradient calculations, for the target shown in Figure 2, over the square survey area (-800m, -700m) to (1200m, 1300m). Contour values are in multiples of 0.01nT/m. The strength of the target magnetization vector μ was set to (1, 1, 1)1.0e05 nT/m and the target thickness parameter was set to $T = 100\text{m}$, giving a total magnetic anomaly of 61.028nT at the observation point (0,0,0).